Letter | Editors' Suggestion

Antibonding ground states in crystal phase quantum dots

Martyna Patera* and Michał Zieliński†

Institute of Physics, Faculty of Physics, Astronomy and Informatics, Nicolaus Copernicus University, ul. Grudziądzka 5, 87-100 Toruń, Poland

(Received 22 March 2022; revised 14 June 2022; accepted 21 June 2022; published 12 July 2022)

Crystal phase quantum dots are formed during the nanowire growth by vertically stacking distinct crystal phases of the same chemical compound. In this Letter we show, using an atomistic many-body approach, that InP crystal phase quantum dots may exhibit a peculiar and rare antibonding hole ground state. Interestingly, even small strains due to a wurtzite–zinc-blende lattice mismatch—which is often neglected—can strongly affect the properties of the lowest hole states, resulting in unusual double-peak features in the excitonic optical spectra.

DOI: 10.1103/PhysRevB.106.L041405

An antibonding ground state is an unusual and rare feature of artificial molecules predicted [1,2] and observed [3,4] in double quantum dots, more recently in photonic crystal molecules [5], and in adatom molecules [6]. It may be argued that the ground state wave function cannot change sign, and thus the ground state cannot be of an antibonding character [7]. However, in semiconductor quantum dot molecules the antibonding ground state stem from the tunneling term and can change sign due to a spin-orbit interaction [3,8,9]. The antibonding hole ground state in artificial molecules therefore differs tremendously from the natural ordering in real diatomic molecules. This is interesting from both a basic research point of view, and in view of potential applications. Such quasimolecular states could in principle allow for wave-function engineering and thus control the magnetic, spin, and optical properties, with possible applications in optics, transport, or quantum information [10], and quantum simulations [5].

In this Letter, we predict, using an atomistic tight-binding approach, that the antibonding hole ground state may in fact emerge in a single crystal phase quantum dot (CPQD) [11] of type-II confinement, which mimics molecularlike behavior [12]. To this aim, we perform a theoretical study of CPQDs formed by an InP zinc-blende (ZB) section sandwiched between two InP wurtzite (WZ) sections, altogether forming a nanowire [11]. We show that the coupling between two sections of wurtzite leads to the formation of quasimolecular states which, for large dot heights and diameters, may be of an antibonding character. Importantly, the formation of antibonding ground states competes with strain, which originates from a small lattice mismatch between different crystal phases. Whereas the actual magnitude of this mismatch is debatable [13–15], even small strains may affect the excitonic spectra, leading to the mixing of antibonding/bonding states and causing unusual double-peak features in the excitonic spectra for CPQDs.

We perform our calculations using the empirical tight-binding method with the sp^3s^* parametrization [12,16–18]. The single-particle tight-binding Hamiltonian for a system of N atoms and m orbitals per atom can be written in the language of the second quantization as follows [19,20],

$$\hat{H}_{\mathrm{TB}} = \sum_{i=1}^{N}\sum_{\alpha=1}^{m} E_{i\alpha} c_{i\alpha}^{+} c_{i\alpha} + \sum_{i=1}^{N}\sum_{\alpha,\beta=1}^{m} \lambda_{i\alpha,\beta} c_{i\alpha}^{+} c_{i\beta} + \sum_{i=1}^{N}\sum_{j=1}^{\text{near. neigh.}}\sum_{\alpha,\beta=1}^{m} t_{i\alpha,j\beta} c_{i\alpha}^{+} c_{j\beta}, \tag{1}$$

where $c_{i\alpha}^{+}$ ($c_{i\alpha}$) is the creation (annihilation) operator of a carrier on the (spin-)orbital α localized on the site i, $E_{i\alpha}$ is the corresponding on-site (diagonal) energy, and $t_{i\alpha,j\beta}$ describes the hopping (off site and off diagonal) of the particle between the orbitals on the four nearest-neighboring sites. Index i iterates over all atoms, whereas j iterates over the four nearest neighbors only. Coupling to further neighbors is thus neglected, and $\lambda_{i\alpha,\beta}$ (on site and off diagonal) accounts for the spin-orbit interaction following the description given by Chadi [16], which includes the contributions from atomic p orbitals. We use the modified Vogl *et al.* [21] set of empirical parameters augmented to account for the spin-orbit interaction [16], the valence band offset (VBO) between the ZB and WZ segments (Fig. 1), the increased band gap, and the presence of crystal-field splitting in the WZ phase [22–25]. The modeling of CPQDs is challenging as the reported values of WZ band-structure parameters vary considerably. For example, published values of InP ZB-WZ VBO range from 45 to 111 meV [23–25]. Here, following Ref. [22], we assume the VBO to be equal to 64.6 meV (Fig. 1), and crystal-field splitting equal to 100 meV [22,24,26]. As the VBO plays an important role in the modeling [27], we are also discussing the VBO dependence.

To account for the electron-hole interaction, we first solve self-consistently a pair of coupled electron-hole tight-binding equations, similar to Ref. [28]. Thus, the Schrödinger equation for the electron is solved in the presence of a Coulomb potential coming from the hole, and vice versa. This forms a

*mpatera@doktorant.umk.pl
†mzielin@fizyka.umk.pl

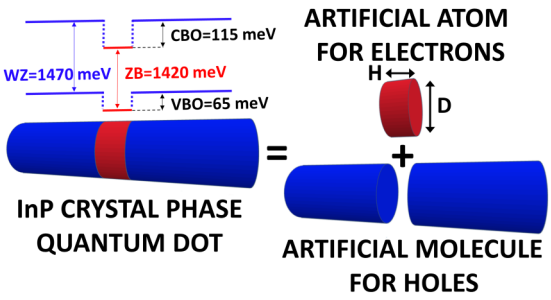

FIG. 1. Schematics of systems under consideration, including the band alignment of InP crystal phases and an illustration of a quasimolecule formed by two wurtzite sections. H and D denote the CPQD height and diameter, respectively.

potentially very time-consuming stage of computation, however, we found that usually only several iterations are needed for a μeV convergence. Next, to account for the effects of configuration mixing and the exchange interaction, the excitonic spectra [29] are calculated with the configuration-interaction method described in detail in Refs. [19,30]. However, the electron and hole states are taken from the self-consistent field (SCF) tight-binding stage of calculation, rather than from the noninteracting single-particle spectra. Preceding the configuration-interaction state with the SCF calculation allows for a much better convergence of many-body spectra. More details of the self-consistent approach (in particular regarding the convergence of calculations) for CPQDs will be described elsewhere. We note that the calculation of the Coulomb matrix elements presents a formidable challenge [31,32]. Here, we benefit from using the latest version of our COULOMBO code [30], which performs highly efficient calculations in the Fourier space [33]. For completeness, we note that the dipole matrix elements are calculated using an approach given in Refs. [19,32]. Finally, in the second part of this Letter, we account for strain effects by using the valence force field method of Keating [2,34–36], with the Harrison scaling law of hopping matrix elements [37]. Minimization of the strain energy is performed with the conjugate gradient method [2,36], whereas strain is incorporated into the Hamiltonian via Slater-Koster rules [38] and the Harrison scaling law of hopping matrix elements [37].

We model CPQDs defined by a ZB InP segment, with the height varying from 1 (single ABC stacking sequence) to 5 nm, grown along the [111] direction, with diameters varying from 12 to 47 nm. The ZB is embedded between two WZ InP segments grown along the [0001] direction as shown schematically in Fig. 1, which also shows the corresponding energy band alignment.

Figures 2(a) and 2(b) show the charge densities of the electron and hole ground state e_1 and h_1, respectively, obtained after the SCF procedure, for a CPQD of ZB section height equal to 2 nm and a diameter of 23.5 nm. The e_1 state is predominately localized in the ZB section, however, with notable tails in both WZ sections. On the contrary, h_1 and h_2 (first excited hole state) are mostly confined in the WZ sections, yet are attracted by the Coulomb interaction from the electron state, as manifested in the confining potential plot

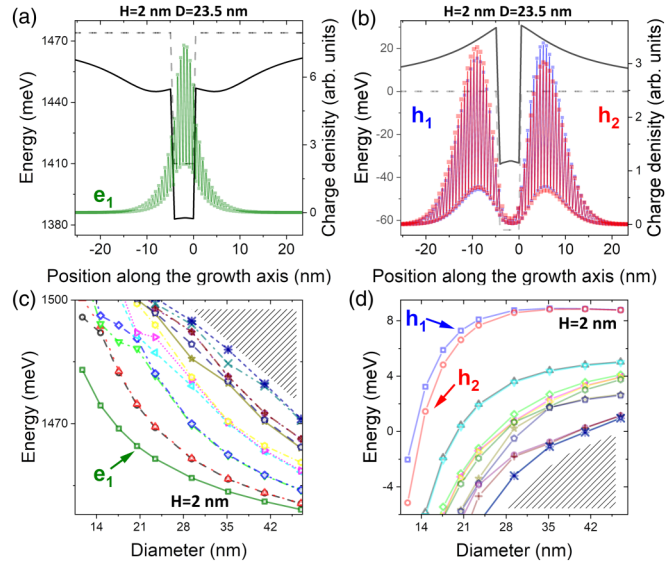

FIG. 2. (a) Electron ground e_1 and (b) hole ground h_1 and first excited state h_2 charge densities, and their respective confining potentials (solid lines) for a CPQD of 2 nm height and diameter of 23.5 nm. The band alignment prior to a self-consistent calculation is shown for comparison (dashed lines). (c) Several lowest electron and (d) hole states for CPQD of $H = 2$ nm as a function of nanowire diameter. Shaded (patterned) areas mark higher excited states.

(black solid line; for comparison the gray dashed line shows band alignment without the Coulomb interaction). States h_1 and h_2 are similar with only some differences in peak heights. The system has C_{3v} symmetry and therefore it lacks the rotoinversion [39] symmetry (in the growth direction) that would disallow such a difference.

The energy spectrum [Fig. 2(c)] of the electron resembles the shell structure of a typical single quantum dot (Fig. 1). The hole spectrum is different [Fig. 2(d)], formed by pairs of quasimolecular states. The splitting between the ground and the first excited state strongly depends on the dot diameter, varying from several meV's for the smallest diameters to 12 μeV for the largest diameter in Fig. 2(d).

By itself, due to the highly oscillatory character of atomistic wave functions, the charge density shown in Fig. 2(b) makes it often very challenging to determine the character of hole states. However, as the electron ground state is of well-defined S symmetry (even parity), thus calculating the optical transition rates for electron-hole recombination allows for an indirect determination of h_1/h_2 hole state symmetries (parities) accordingly. Therefore, in Fig. 3, we study the optical activity of the two lowest excitonic branches. These are formed from electron-hole configurations dominated by e_1/h_1 and e_1/h_2 contributions, respectively. Each of the branches actually consists of four states: two bright and two dark states (due to spin selection rules). These states are doubly degenerate, as there is no fine-structure splitting in C_{3v} systems. The spin-allowed states may still be optically inactive should the transition dipole moment between the electron state and the hole state vanish. Such behavior, by symmetry, is expected for the s-like electron ground state and antibonding hole states, as they have different parity. Thus, the vanishing optical activity

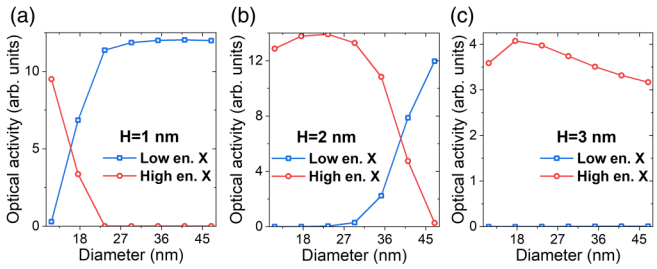

FIG. 3. Optical activity of the two lowest excitonic branches as a function of diameter, and for three different heights (a)–(c). For $H =$ 3 nm the lower excitonic state (blue squares) is optically nonactive for all diameters, indicating the antibonding character of the hole states. For other heights a more complicated behavior is possible with either a higher excitonic branch (red circles) being optically active or both states interchanging their brightness.

of e_1/h_1 states is a direct indicator of an antibonding hole ground state.

As shown in Fig. 3 for a larger dot height (3 nm), the lowest excitonic branch remains optically inactive for a broad range of diameters, indicating the antibonding character of the hole ground state, whereas the higher excitonic branch has strong optical activity. For a smaller height CPQD of 2 nm the antibonding ground state dominates for diameters up to 27 nm. For an even smaller dot of 1 nm the situation is reversed: Flat, high-diameter CPQDs have a bonding, optically active hole ground state. However, in small height (1 nm) and small diameter (13.7 nm) systems, the hole ground state again appears to be antibonding.

Figure 4 shows results of calculations for CPQDs with five different heights and seven various diameters. To make the comparison feasible, we show results in the form of a contour plot. First, for completeness, we show [Fig. 4(a)] the excitonic ground state energy that reveals a strong monotonic dependence with a reduction of both height and diameter. A stronger dependence on height is related to a stronger vertical confinement of the electron in the ZB section.

Next, we study [Fig. 4(b)] a contour plot of h_1/h_2 splitting with color saturation proportional to the splitting magnitude, and the choice of color (blue/red) indicating the character of the hole ground state. As shown in Fig. 4(b), and consistent with Fig. 3, the large height/small diameter systems

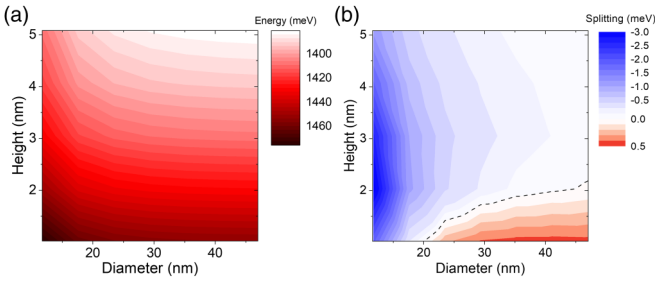

FIG. 4. Contour plots illustrating the size dependence of (a) the excitonic ground state energy and (b) the two lowest hole states' (h_1 and h_2) energy splitting. The dashed line separates a negative (blue) splitting region (with the antibonding state hole ground state), from a positive (red) splitting area (the bonding hole ground state).

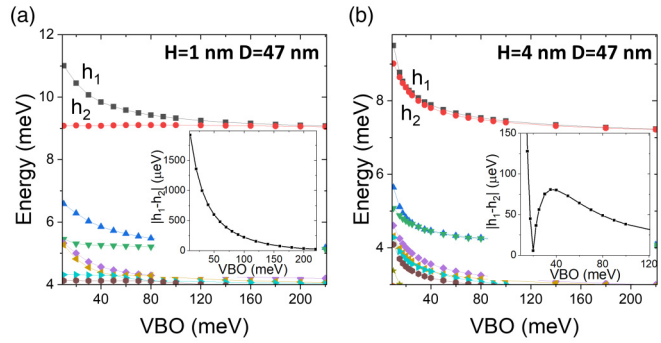

FIG. 5. Energies of the two lowest hole states h_1 and h_2, and their energy splitting (insets) as a function of valence band offset, for two CPQDs of notably different heights: (a) 1 nm and (b) 4 nm, and the same diameter (47 nm). For a flat system (a), in the range of considered VBO values, the h_1 does not cross with h_2, and h_1 remains of bonding character. However, a tall quantum dot (b), manifests a(n) (anti)crossing of hole states occurring at a small VBO of 20 meV. For larger VBO values the ground-hole state is antibonding.

should have an antibonding hole ground state, whereas small height/large diameter dots will have a bonding hole ground state. The dependence of the splitting of the two lowest hole states on a dot radius and diameter is consistent with a picture of CPQD as a system formed by hole states residing in two WZ sections, and coupled via the ZB region. The magnitude of this coupling thus changes with barrier width, although not monotonically, as can be seen in the upper left-hand corner of Fig. 4(b), reaching a maximum for 2–3 nm.

In this spirit, the splitting between the two lowest states should also be expected to depend on the ZB barrier height, i.e., the valence band offset (VBO). Unless specified otherwise, we assume VBO equal to 64.6 meV [22]. However, we can study the effect on the hole spectrum by artificially changing the VBO value as shown in Fig. 5. The increasing VBO value leads to an increased hole barrier height, and thus it reduces the hole splitting [Fig. 5(a)]. For the flat, 1 nm height system, the h_1 state is of a bonding character, and it is far more affected by the VBO choice than the antibonding state h_2. This is consistent with a simplified understanding of a bonding orbital as having a larger charger density in between two main peaks, i.e., in the barrier. Next, for a larger height dot of 4 nm, the hole level splittings are far smaller due to a decreased coupling through a thicker ZB barrier. Moreover, the overall trend is more complicated, with h_1/h_2 levels undergoing an apparent crossing (see the inset of Fig. 5) at VBO equal to 20 meV. A similar crossing is also observed for dots of 2 and 3 nm (for VBO of 35 and 30 meV, respectively; assuming the same diameter of 47 nm). Thus, despite a broad range of possible VBO values reported in the literature, the antibonding state is expected to robustly occur for larger height CPQDs.

Strain effects in CPQDs are often neglected or assumed very low [11,12,40]. Several authors report an InP ZB/WZ lattice mismatch from 0.2% to approximately 1% [13–15], thus in fact very small compared to InAs/GaAs dots. Nonetheless, strain affects the bulk-band structure via relatively large deformation potentials [41]. Thus, even small

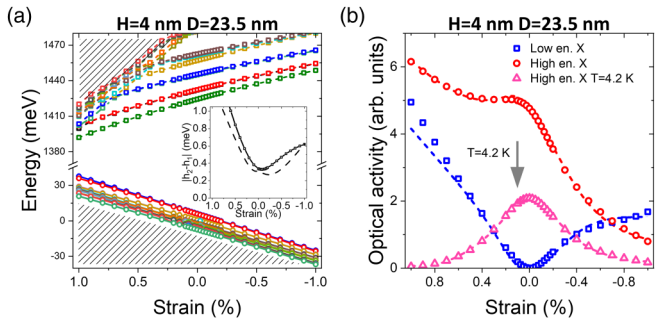

FIG. 6. Impact of strain on (a) electron and hole spectra and (b) optical activity of the two lowest excitonic branches including also the effect of temperature. Dashed lines are a fit to a model discussed in the text. The strain goes from tensile (positive sign) to compressive (negative sign). The inset in (a) shows the lowest two hole levels splitting the strain evolution, compared with a fit to a model (black dashed line).

strain could lead to substantial energy shifts. Figure 6(a) shows the effect of strain on the electron and hole spectra. We assume a larger lattice constant, and thus a compressive (negative) strain in the ZB area. For completeness, we also study a case with a smaller ZB constant leading to a tensile (positive) strain. Either way the compressive/tensile strain leads to an overall blue/redshift of electron energies, respectively. Strain can also penetrate outside of the dot [42], and thus shift hole energies as well. In effect, we observe an overall shift of the excitonic ground energy of 57 meV for -1% (compressive) strain for an $H = 4$ nm and $D = 23.5$ nm system, with even larger shifts (80–90 meV) for smaller systems. Similar, though of opposite sign, shifts are observed for tensile strain. For large tensile strain, there is a rapid reduction of higher electron bands consistent with a discussion presented in Ref. [43], with a possible reversal of the energy ordering for higher tensile strains and increased dot diameter. Since there are no expectations regarding strong strain at the ZB-WZ interface [13–15,43], thus we do not study strains outside of the -1% to 1% region. Nonetheless, even small strain strongly modifies the electron and hole spectra, thus, the actual magnitude of strain and VBO must be known far more accurately, aiming for a better agreement of the theoretical results with CPQD experiments.

We also found that strain strongly affects the excitonic optical spectra, as illustrated in Fig. 6(b). For a nonstrained system the low excitonic branch has a vanishing oscillator strength indicating an antibonding hole state. With increasing strains both branches apparently start to "swap" their optical activities. For large compressive strains the optical activity of the lower branch can even dominate. This indicates a strong mixing of bonding and antibonding states due to strain.

In a typical photoluminescence experiment the optical activity of excitons is also affected by temperature which determines the populations of the excitonic states [44]. In usual (type-I) quantum dots, the energy level spacings are so large that in low-temperature (4.2 K) experiments the higher states remain unoccupied, and are thus optically inactive. For CPQDs the energy spacings between hole levels are much smaller. However, with $T = 4.2$ K (and kT product equal to

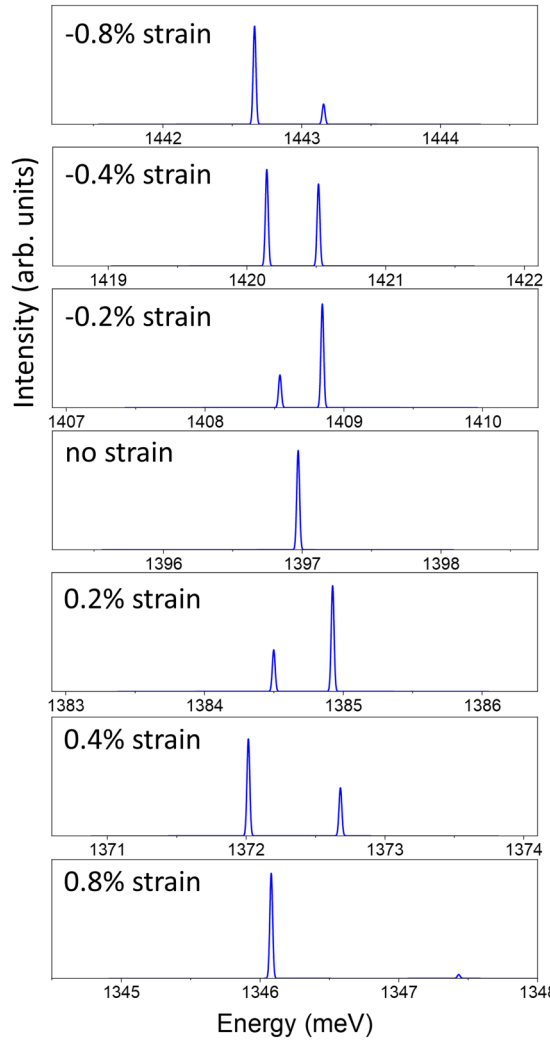

FIG. 7. Excitonic emission spectra of a CPQD with $H = 4$ nm and $D = 23.5$ nm as a function of strain. The compressive strain corresponds to negative signs, whereas the tensile strain is positive. For intermediate strains the double-peak structure emerges, as a result of bonding/antibonding mixing.

0.36 meV) the reduction of the probability of occupation of the higher excitonic branch (and the optical activity) is notable. The inclusion of temperature is thus shown on Fig. 6(b) (magenta triangles) showing a pronounced dumping of the higher branch optical activity.

To further understand the role of strain we are utilizing a simple model neglecting the exchange and configuration mixing effects. The excitonic Hamiltonian is given in terms of two basis functions associated with the left $|L\rangle = |e_1\rangle|h_L\rangle$ and right $|R\rangle = |e_1\rangle|h_R\rangle$ parts of CPQD, with e_1 being the electron state. In this basis the Hamiltonian has a 2×2 form,

$$H_{LR} = \begin{bmatrix} E_L & t \\ t & E_R \end{bmatrix} = \begin{bmatrix} E & t \\ t & E + \Delta \end{bmatrix}, \tag{2}$$

with E the (excitonic) energy, t being the hopping term responsible for the (hole) coupling between the left and right wurtzite sections through the zinc-blende barrier, and Δ is the energy difference between the left and right section. Small

strains can be included into modeling by assuming a linear strain dependence,

$$H_{LR}^{\text{strain}} = \begin{bmatrix} E + a_L\epsilon & t + a_{LR}\epsilon \\ t + a_{LR}\epsilon & E + \Delta + a_R\epsilon \end{bmatrix}, \tag{3}$$

where ϵ is the strain, and a_L, a_R are coefficients (deformation potentials) responsible for energy shifts of the left and right (WZ) sections, respectively, which can be different due to a lack of inversion symmetry. a_{LR} describes the change of hopping due to a variation of barrier height caused by strain (strained band offset).

The Hamiltonian of Eq. (2) can also be rewritten in the antibonding/bonding (AB) basis:

$$H_{AB} = \begin{bmatrix} E + t + \frac{\Delta}{2} & -\frac{\Delta}{2} \\ -\frac{\Delta}{2} & E - t + \frac{\Delta}{2} \end{bmatrix}. \tag{4}$$

Similarly, Eq. (3) can be reexpressed in the AB basis,

$$H_{AB}^{\text{strain}} = H_{AB} + \epsilon \begin{bmatrix} a_A & a_{AB} \\ a_{AB} & a_B \end{bmatrix}, \tag{5}$$

where H_{AB} is the unstrained Hamiltonian, $a_{A/B} = (a_L + a_R \mp 2a_{LR})/2$ describe deformation potentials of the antibonding/bonding states, respectively, whereas $a_{AB} = (a_L - a_R)/2$ is a strain-related bonding-antibonding mixing term. We can find these parameters by fitting to the atomistic results with $E = 1397.221\,\text{meV}$, $t = 0.156\,\text{meV}$, $\Delta = -0.056\,\text{meV}$, with $a_A = -57.48\,\text{meV}$, $a_B = -56.99\,\text{meV}$, $a_{AB} = 0.271\,\text{meV}$ for compressive strain, and $a_A = -57.206\,\text{meV}$, $a_B = -57.26\,\text{meV}$, $a_{AB} = 0.669\,\text{meV}$ for tensile strain.

Results of the fitting are shown as dashed lines in Fig. 6(b) closely matching the atomistic targets, where we also accounted for the temperature effect in an occupation probability of the higher branch [45]. The corresponding lowest hole level splitting is shown as a dashed line on inset in Fig. 6(a). However, due to model simplicity, it cannot be simultaneously fit with the same accuracy as the optical activity.

Finally, to better illustrate the strain evolution of CPQD emission intensity, Fig. 7 yet again shows the optical spectra, this time in the form of photoluminescence peaks, with the effect of temperature included, and with accounting for finite linewidths (10 μeV). Without strain, a single line in the spectra is present, due to emission from the higher (bonding) excitonic branch, whereas the ground exciton branch (antibonding) remains inactive. Contrarily, for strain higher than 0.8% (both tensile and compressive) the emission is dominated by the lower excitonic branch of a bonding hole state character, with a systematically vanishing contribution from a higher (antibonding) branch. This term is further quenched by increasing the energy spacing from the ground state, and thus decreasing the probability of a higher state occupation. For an intermediate range of strain, a characteristic [12] pattern of double peaks emerges in the spectra, with either a pronounced low-energy peak and a dominating higher-energy peak (for $\pm 0.2\%$ strain) or a peculiar structure of two peaks of comparable heights (-0.4%).

To summarize, a CPQD can host an unusual antibonding hole ground state which leads to a vanishing optical activity of a lowest excitonic manifold. However, the spectra of CPQD may strongly depend on their dimension, and ZB-WZ lattice mismatch, with a mixing of antiboding/bonding states, and the onset of characteristic double-peak features. Finally, we note that further research is needed to determine the strain and band offsets in ZB-WZ mixed systems.

M.Z. acknowledges support from the Polish National Science Centre based on Decision No. 2018/31/B/ST3/01415.

[1] W. Jaskólski, M. Zieliński, and G. W. Bryant, Coupling and strain effects in vertically stacked double inas/gaas quantum dots: Tight-binding approach, Acta Phys. Pol., A **106**, 193 (2004).

[2] W. Jaskólski, M. Zieliński, G. W. Bryant, and J. Aizpurua, Strain effects on the electronic structure of strongly coupled self-assembled InAs/GaAs quantum dots: Tight-binding approach, Phys. Rev. B **74**, 195339 (2006).

[3] M. F. Doty, J. I. Climente, M. Korkusinski, M. Scheibner, A. S. Bracker, P. Hawrylak, and D. Gammon, Antibonding Ground States in InAs Quantum-Dot Molecules, Phys. Rev. Lett. **102**, 047401 (2009).

[4] A. I. Yakimov, V. Timofeev, A. Nikiforov, and A. V. Dvurechenskii, Antibonding ground state of holes in double vertically coupled Ge/Si quantum dots, JETP Lett. **94**, 744 (2012).

[5] N. Caselli, F. Intonti, F. Riboli, A. Vinattieri, D. Gerace, L. Balet, L. H. Li, M. Francardi, A. Gerardino, A. Fiore, and M. Gurioli, Antibonding ground state in photonic crystal molecules, Phys. Rev. B **86**, 035133 (2012).

[6] Y. Marques, A. E. Obispo, L. S. Ricco, M. de Souza, I. A. Shelykh, and A. C. Seridonio, Antibonding ground state of adatom molecules in bulk Dirac semimetals, Phys. Rev. B **96**, 041112(R) (2017).

[7] R. P. Feynman and M. Cohen, The energy spectrum of the excitations in liquid helium, Appendix A: Proof of non-degeneracy of the ground state, Ph.D. thesis, California Institute of Technology, 1956, https://thesis.library.caltech.edu/1007/1/Cohen_m_1956.pdf.

[8] J. Planelles, J. I. Climente, F. Rajadell, M. F. Doty, A. S. Bracker, and D. Gammon, Effect of strain and variable mass on the formation of antibonding hole ground states in InAs quantum dot molecules, Phys. Rev. B **82**, 155307 (2010).

[9] T. Chwiej and B. Szafran, Signatures of antibonding hole ground states in exciton spectra of vertically coupled quantum dots in an electric field, Phys. Rev. B **81**, 075302 (2010).

[10] K. Sablon, Artificial molecules: Antibonding molecular ground state for holes revealed, Nanoscale Res. Lett. **4**, 191 (2009).

[11] N. Akopian, G. Patriarche, L. Liu, J.-C. Harmand, and V. Zwiller, Crystal phase quantum dots, Nano Lett. **10**, 1198 (2010).

[12] M. Bouwes Bavinck, K. D. Jöns, M. Zieliński, G. Patriarche, J.-C. Harmand, N. Akopian, and V. Zwiller, Photon cascade from a single crystal phase nanowire quantum dot, Nano Lett. **16**, 1081 (2016).

[13] D. Kriegner, E. Wintersberger, K. Kawaguchi, J. Wallentin, M. T. Borgström, and J. Stangl, Unit cell parameters of wurtzite InP nanowires determined by x-ray diffraction, Nanotechnology **22**, 425704 (2011).

[14] L. C. Dacal and A. Cantarero, Ab initio electronic band structure calculation of InP in the wurtzite phase, Solid State Commun. **151**, 781 (2011).

[15] P. Faria Junior and G. Sipahi, Band structure calculations of InP wurtzite/zinc-blende quantum wells, J. Appl. Phys. **112**, 103716 (2012).

[16] D. J. Chadi, Spin-orbit splitting in crystalline and compositionally disordered semiconductors, Phys. Rev. B **16**, 790 (1977).

[17] S. Lee, F. Oyafuso, P. von Allmen, and G. Klimeck, Boundary conditions for the electronic structure of finite-extent embedded semiconductor nanostructures, Phys. Rev. B **69**, 045316 (2004).

[18] M. Zieliński, Multi-scale simulations of semiconductor nanostructures, Acta Phys. Pol., A **122**, 312 (2012).

[19] M. Zieliński, M. Korkusinski, and P. Hawrylak, Atomistic tight-binding theory of multiexciton complexes in a self-assembled InAs quantum dot, Phys. Rev. B **81**, 085301 (2010).

[20] M. Zieliński, Including strain in atomistic tight-binding Hamiltonians: An application to self-assembled InAs/GaAs and InAs/InP quantum dots, Phys. Rev. B **86**, 115424 (2012).

[21] P. Vogl, H. P. Hjalmarson, and J. D. Dow, A semi-empirical tight-binding theory of the electronic structure of semiconductors, J. Phys. Chem. Solids **44**, 365 (1983).

[22] A. De and C. E. Pryor, Predicted band structures of III-V semiconductors in the wurtzite phase, Phys. Rev. B **81**, 155210 (2010).

[23] M. Murayama and T. Nakayama, Chemical trend of band offsets at wurtzite/zinc-blende heterocrystalline semiconductor interfaces, Phys. Rev. B **49**, 4710 (1994).

[24] F. Bechstedt and A. Belabbes, Structure, energetics, and electronic states of III–V compound polytypes, J. Phys.: Condens. Matter **25**, 273201 (2013).

[25] J.-M. Jancu, K. Gauthron, L. Largeau, G. Patriarche, J.-C. Harmand, and P. Voisin, Type II heterostructures formed by zinc-blende inclusions in InP and GaAs wurtzite nanowires, Appl. Phys. Lett. **97**, 041910 (2010).

[26] L. Zhang, J.-W. Luo, A. Zunger, N. Akopian, V. Zwiller, and J.-C. Harmand, Wide InP nanowires with wurtzite/zincblende superlattice segments are type-II whereas narrower nanowires become type-I: An atomistic pseudopotential calculation, Nano Lett. **10**, 4055 (2010).

[27] M. Zieliński, Valence band offset, strain and shape effects on confined states in self-assembled InAs/InP and InAs/GaAs quantum dots, J. Phys.: Condens. Matter **25**, 465301 (2013).

[28] Y. M. Niquet, Electronic and optical properties of InAs/GaAs nanowire superlattices, Phys. Rev. B **74**, 155304 (2006).

[29] P. Hawrylak and M. Korkusiński, in *Single Quantum Dots Fundamentals, Applications and New Concepts*, edited by P. Michler, Topics in Applied Physics Vol. 90 (Springer, New York, 2003).

[30] P. T. Różański and M. Zieliński, Efficient computation of Coulomb and exchange integrals for multi-million atom nanostructures, Comput. Phys. Commun. **238**, 254 (2019).

[31] S. Lee, L. Jönsson, J. W. Wilkins, G. W. Bryant, and G. Klimeck, Electron-hole correlations in semiconductor quantum dots with tight-binding wave functions, Phys. Rev. B **63**, 195318 (2001).

[32] S. Schulz, S. Schumacher, and G. Czycholl, Tight-binding model for semiconductor quantum dots with a wurtzite crystal structure: From one-particle properties to Coulomb correlations and optical spectra, Phys. Rev. B **73**, 245327 (2006).

[33] P. T. Różański and M. Zieliński, Linear scaling approach for atomistic calculation of excitonic properties of 10-million-atom nanostructures, Phys. Rev. B **94**, 045440 (2016).

[34] P. N. Keating, Effect of invariance requirements on the elastic strain energy of crystals with application to the diamond structure, Phys. Rev. **145**, 637 (1966).

[35] R. M. Martin, Elastic properties of ZnS structure semiconductors, Phys. Rev. B **1**, 4005 (1970).

[36] T. Saito and Y. Arakawa, Electronic structure of piezoelectric $In_{0.2}Ga_{0.8}N$ quantum dots in GaN calculated using a tight-binding method, Physica E **15**, 169 (2002).

[37] W. A. Harrison, *Electronic Structure and the Properties of Solids* (Freeman, New York, 1980).

[38] J. C. Slater and G. F. Koster, Simplified LCAO method for the periodic potential problem, Phys. Rev. **94**, 1498 (1954).

[39] R. Singh and G. Bester, Nanowire Quantum Dots as an Ideal Source of Entangled Photon Pairs, Phys. Rev. Lett. **103**, 063601 (2009).

[40] M. Taherkhani, M. Willatzen, J. Mørk, N. Gregersen, and D. P. S. McCutcheon, Type-II quantum-dot-in-nanowire structures with large oscillator strength for optical quantum gate applications, Phys. Rev. B **96**, 125408 (2017).

[41] I. Vurgaftman, J. R. Meyer, and L. R. Ram-Mohan, Band parameters for III–V compound semiconductors and their alloys, J. Appl. Phys. **89**, 5815 (2001).

[42] C. Pryor, J. Kim, L. W. Wang, A. J. Williamson, and A. Zunger, Comparison of two methods for describing the strain profiles in quantum dots, J. Appl. Phys. **83**, 2548 (1998).

[43] O. Marquardt, M. Ramsteiner, P. Corfdir, L. Geelhaar, and O. Brandt, Modeling the electronic properties of GaAs polytype nanostructures: Impact of strain on the conduction band character, Phys. Rev. B **95**, 245309 (2017).

[44] E. Dekel, D. V. Regelman, D. Gershoni, E. Ehrenfreund, W. V. Schoenfeld, and P. M. Petroff, Cascade evolution and radiative recombination of quantum dot multiexcitons studied by time-resolved spectroscopy, Phys. Rev. B **62**, 11038 (2000).

[45] Additionally, we fit the total optical activity ($|M|^2$) to atomistic calculations as well.